Electronic Supplementary Material (ESI) for Green Chemistry.

Supporting Information

Boosting CO production from visible-light CO_2 photoreduction via defects induced electronic structure tuning and reaction energy optimization on ultrathin carbon nitride

Jiaying Li,[1,2] Chengxuan He,[1,2] Jinlong Wang,[1,2] Xiaoyi Gu,[1,2] Zehan Zhang,[1,2] Huizi Li, [1,2] Mingyang Li,[1,2] Lingzhi Wang,[1,2] Shiqun Wu,[1,2*] and Jinlong Zhang[1,2,*]

[1]Key Laboratory for Advanced Materials, Joint International Research Laboratory of Precision Chemistry and Molecular Engineering, Feringa Nobel Prize Scientist Joint Research Center, School of Chemistry and Molecular Engineering, East China University of Science & Technology, Shanghai 200237, China

[2]Shanghai Engineering Research Center for Multi-media Environmental Catalysis and Resource Utilization, East China University of Science and Technology, Shanghai 200237, China

*Correspondence: wushiqun@ecust.edu.cn (S. W.)

*Correspondence: jlzhang@ecust.edu.cn (J. Z.)

Experimental Section

Materials:

All materials were used as analytical grade and without further refinement. Urea (99%) and formaldehyde (37 wt. % in H_2O) were purchased from Shanghai Macklin Biochemical Technology Co., Ltd; Ar (99.999 %) and CO_2 (99.999 %) were obtained from the Shanghai Haoqi Gases Company. Deionized water (H_2O, 18.25 MΩ·cm) supplied by an UP Water Purification System was used in the whole experimental processes.

Characterization:

The XRD patterns were obtained using a Rigaku D/MAX diffractometer equipped with Cu Kα radiation (λ = 1.5406 Å). Scanning electron microscopy (SEM) analysis was performed using a TESCAN nova III scanning electron microscope. Diffuse reflectance infrared Fourier transform spectroscopy (DRIFTS) was recorded on Thermo Nicolet is50 at a resolution of 0.09 cm^{-1}. The morphologies of the synthesized samples were examined using HRTEM (JEM-2100), TEM (JEM-1400), and STEM (Tolas). XPS analysis was performed on an ARL Quant X-ray photoelectron spectrometer with Al Kα X-ray (hv = 1486.6 eV) excitation. EPR spectra were collected by a Bruker EMX-8/2.7 instrument. The UV-vis absorption spectra were recorded on a Varian Cary 500 spectrophotometer, employing $BaSO_4$ as a reflectance sample. Raman spectra were acquired using a micro-Raman system (Renishaw in Via-Reflex). PL spectra were measured on a luminescence spectrometry (Cary Eclipse) at room temperature. Time-resolved fluorescence decay spectra were obtained using an FLS 980 spectrometer (EDINBURGH INSTRUMENTS). The surface area was determined by N_2 adsorption at 77 K using an ASAP2020 instrument. CO_2 adsorption-desorption isotherms were obtained on a Micromeritics ASAP 2020 instrument.

Electrochemical tests:

The electrochemical measurements were conducted using an electrochemical analyzer (Zahner, Zennium) at room temperature. The standard three-electrode system comprised a working electrode, a graphite carbon rod serving as the counter electrode, and a saturated calomel electrode used as the reference electrode. The working electrode was prepared by depositing a sample film onto a fluoridetin oxide (FTO) substrate. Typically, 5 mg of photocatalysts were dispersed in 0.5 mL of ethanol, and then 0.02 mL of the solution was dip-coated onto the FTO surface. The coated film was allowed to dry under atmospheric conditions at room temperature.

The resulting film had a fixed area of 1 cm^2. The transient photocurrent responses of the different samples were measured in a N_2-saturated 0.5 M Na_2SO_4 aqueous solution under irradiation from a 300 W Xe lamp. The data of electrochemical impedance spectroscopy (EIS) were obtained in the frequency range from 100 kHz to 0.1 Hz under amplitude of 10 mV using N_2 saturated potassium ferricyanide mixed electrolyte without Xe lamp irradiation. Mott-Schottky (MS) experiments were performed at a frequency of 1 kHz using a N_2-saturated 0.5 M Na_2SO_4 aqueous solution as the electrolyte under dark conditions.

In Situ FT-IR Measurement:

In order to monitor the reaction intermediates of CO_2 photocatalysis, specifically the formation of CO and CH_4, in situ Fourier-transform infrared spectroscopy (FTIR) measurements were performed using a Bruker infrared spectrometer (Tensor II) equipped with a liquid nitrogen-cooled mercury-cadmium-telluride (MCT) detector. Prior to the test, the sample was purged with nitrogen for 1 hour to remove any gases adsorbed on the surface. Subsequently, a mixed gas of CO_2 and water vapor was introduced into the reactor. Following a 30-minute dark treatment period, the photocatalytic reaction was initiated, and IR spectra were recorded simultaneously at regular intervals.

Theoretical calculations: Density functional theory (DFT) is performed using the Dmol3 program of Materials Studio, the ultrasoft pseudopotential was used for electron-ion interactions, and the Perdew-Burke-Ernzerhof (PBE) of the generalized gradient approximation (GGA) was employed to describe the exchange-correlation functional.[1-4] The band structures and the electrostructure calculation was carried by HSE with a 3×3×1 k-point grid for Brillouin zone. The cutoff energy for the plane-wave basis set is set to 400 eV. A vacuum layer of 20 Å is added perpendicular to the sheet to avoid artificial interaction between periodic images. The convergence criterion for the electronic self-consistent iteration and force was set to 10^{-5} eV and 0.01 eV/Å, respectively. The adsorption energy (Eads) of the surface species is defined by $E_{ads}=E_{total}-E_{surface}-E_{species}$, where E_{total} represents the total energy of the adsorbed species with catalyst surface, $E_{surface}$ is the energy of the empty surface, and $E_{species}$ is the energy of the species in the gas phase.

Moreover, the change Gibbs free energy (ΔG) of each species can be obtained from the following equation:

$$(1)\quad \Delta G = \Delta E_{DFT} + \Delta E_{ZPE} - \Delta TS$$

where ΔE_{DFT} is the electronic energy calculated from DFT calculations, ΔE_{ZPE} is the zero-point energy the adsorbed species and ΔS is the entropy contribution at room temperature, respectively.

Results and discussion

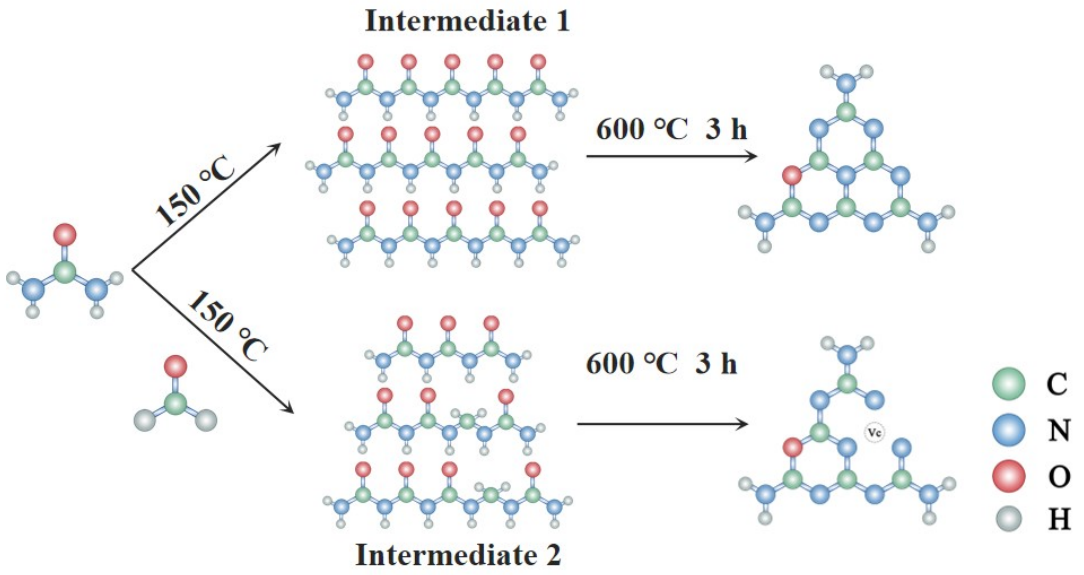

Fig. S1 Schematic illustration of the synthesis route and chemical structure of carbon-deficient and oxygen-doped g-C_3N_4.

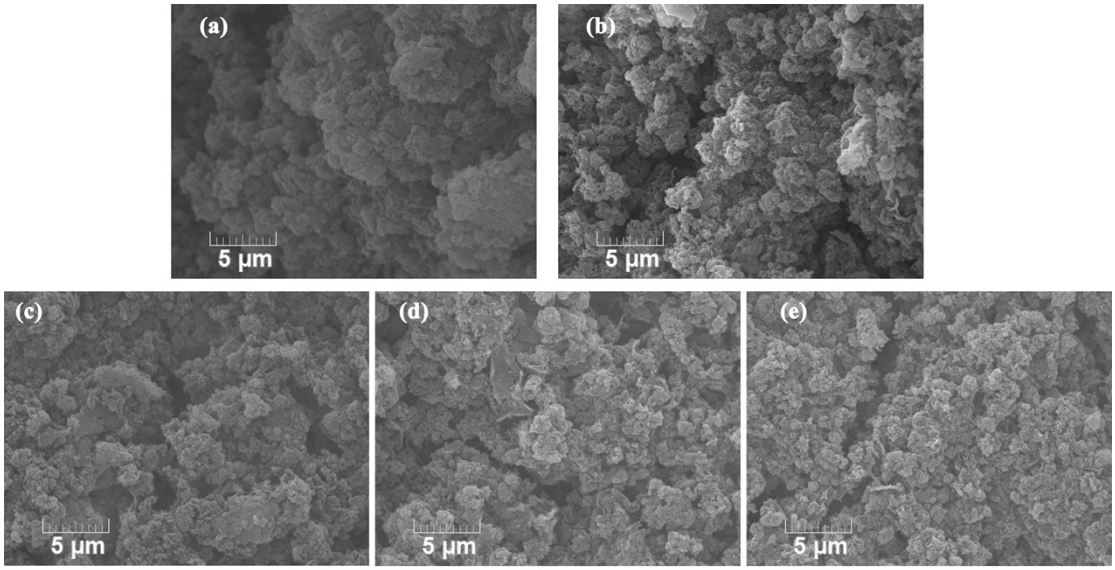

Fig. S2 SEM images of (a) GCN, (b) OCN, (c) Vc-OCN_5, (d) Vc-OCN_{15}, (e) Vc-OCN_{50}.

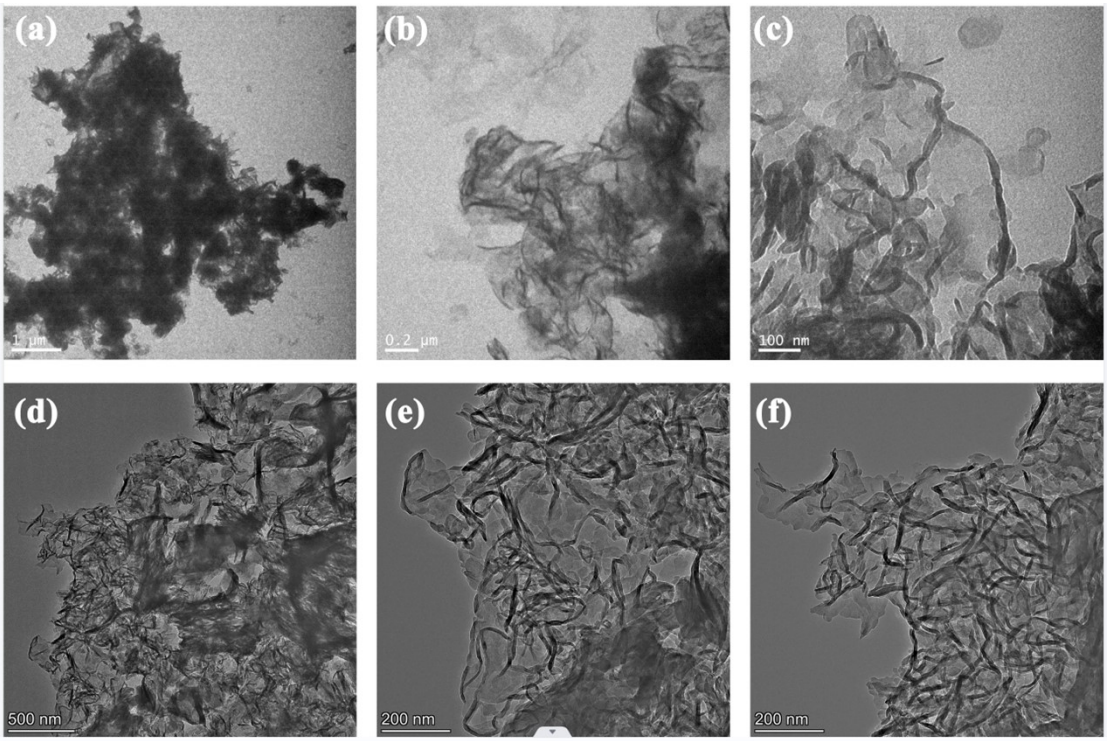

Fig. S3 TEM images of (a) GCN, (b) OCN, (c, d, e, f) Vc-OCN_{15}.

Fig. S4 AFM images of GCN.

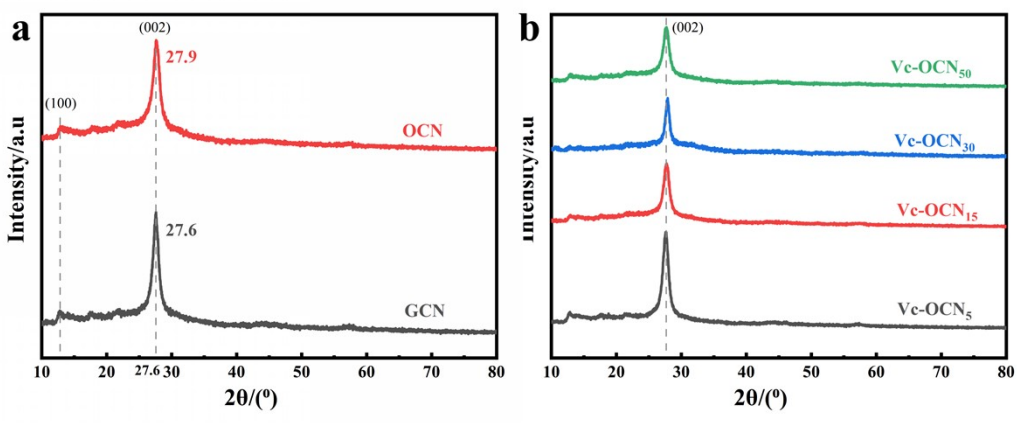

Fig. S5 XRD patterns of GCN, OCN, Vc-OCN_5, Vc-OCN_{15}, Vc-OCN_{30}, Vc-OCN_{50}.

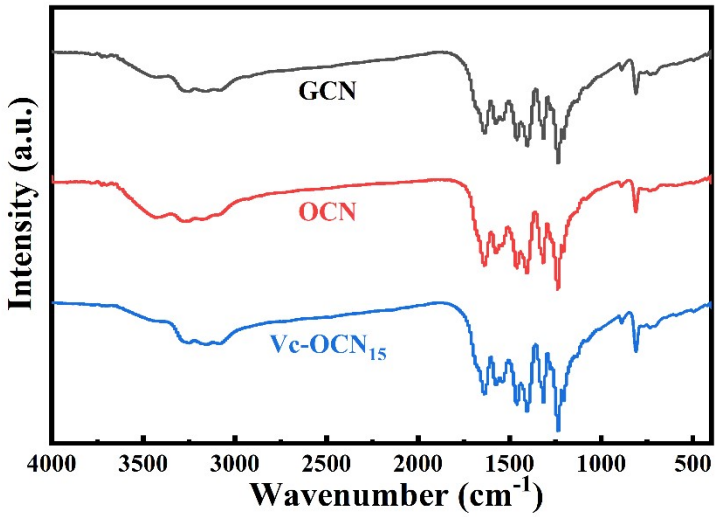

Fig. S6 FT-IR spectra of GCN, OCN, VC-OCN_{15}.

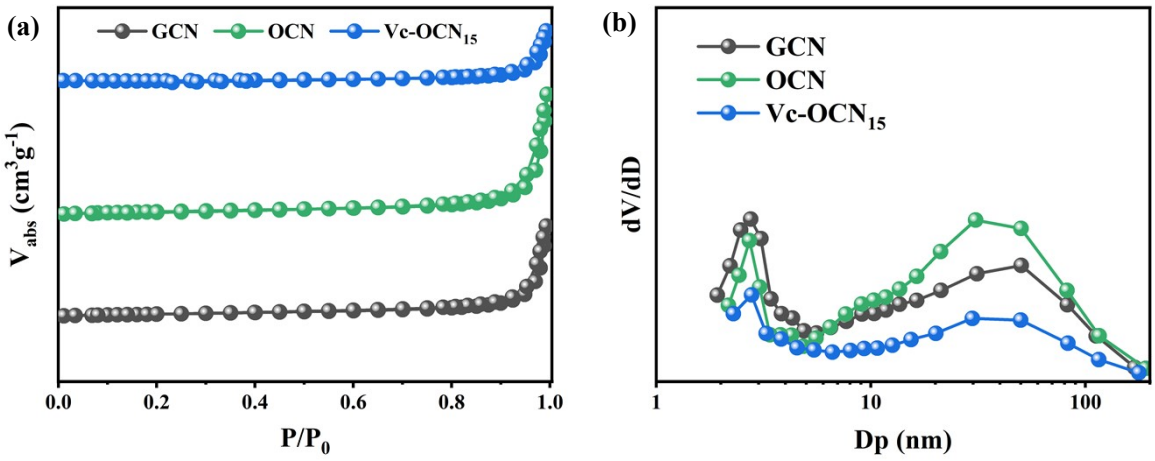

Fig. S7 (a) Nitrogen gas adsorption/desorption isotherms and (b) BJH pore size distribution curves of GCN, OCN and Vc-OCN_{15}.

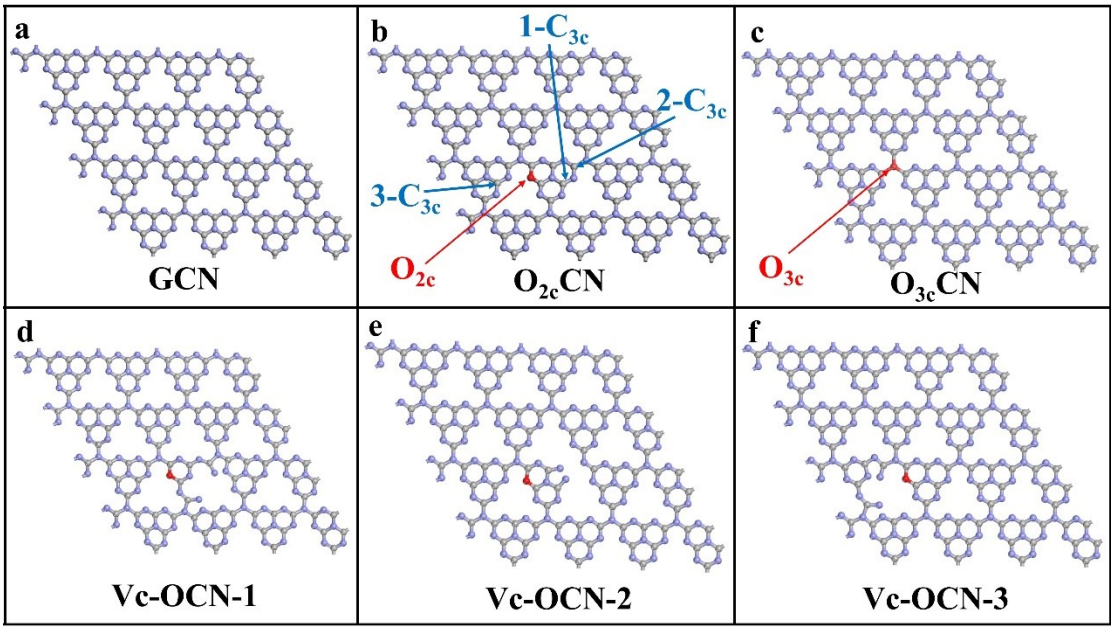

Fig. S8 The optimized DFT model of GCN, OCN, Vc-OCN with different sites of oxygen doping carbon vacancies. The blue, red, and grey ball represent N, O, C atom, respectively.

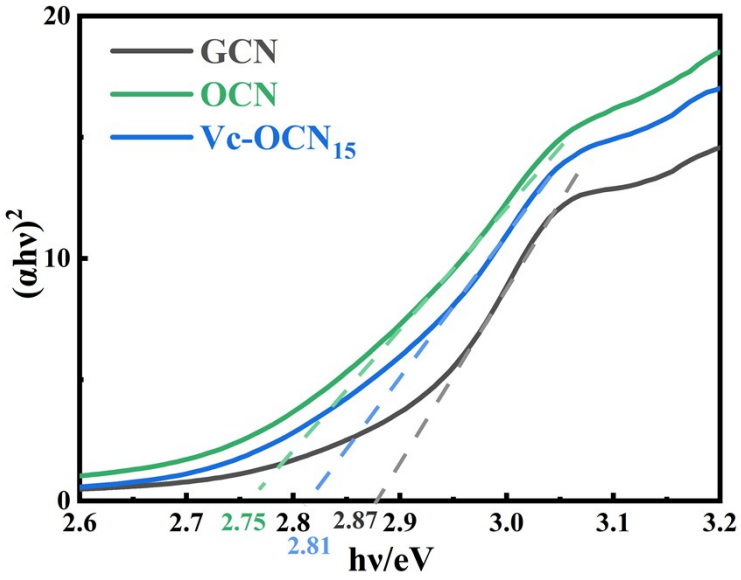

Fig. S9 Tauc plot of GCN, OCN, Vc-OCN_{15}.

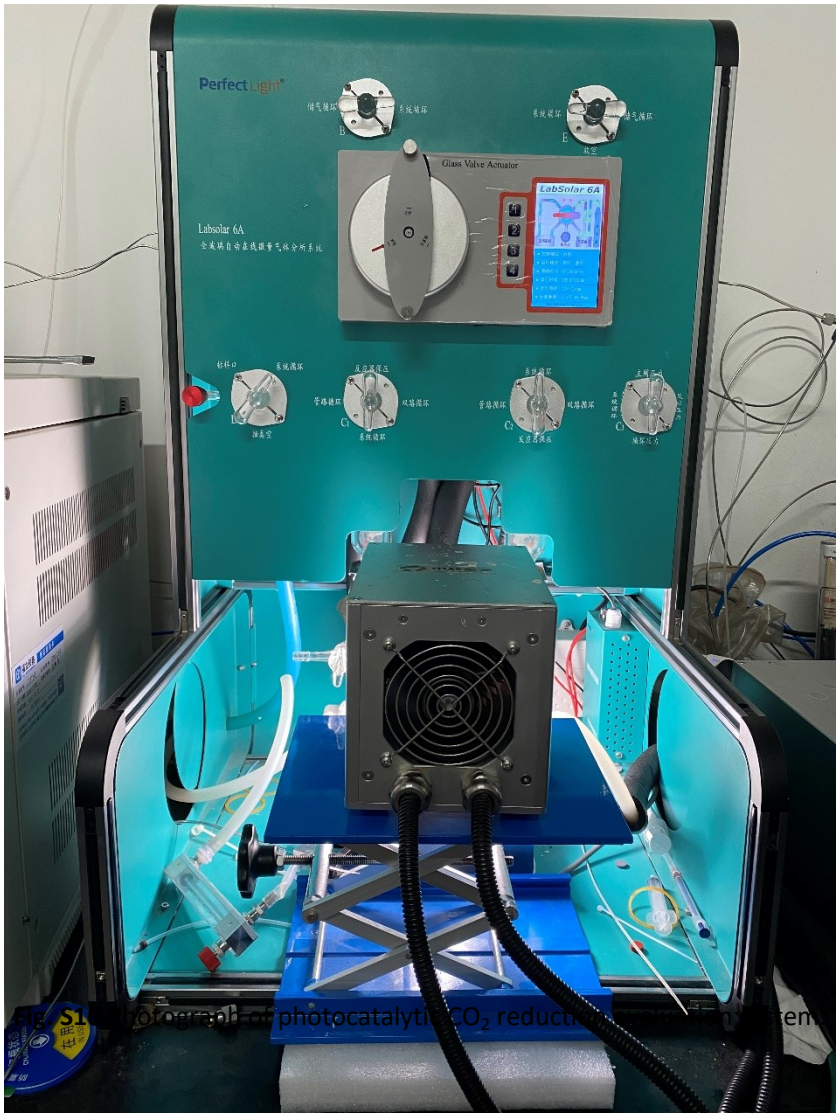

Fig. S1. Photograph of photocatalytic CO_2 reduction reaction system.

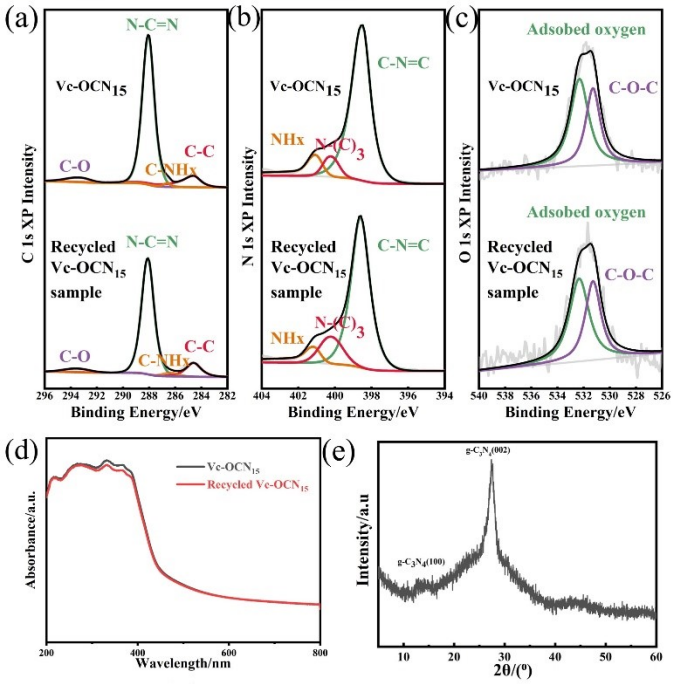

Fig. S11 The (a) C 1s, (b) N 1s, and (c) O 1s high resolution XPS spectra of Vc-OCN_{15}, Recycled Vc-OCN_{15} ;(d) The UV-vis DRS spectra of Vc-OCN_{15}, Recycled Vc-OCN_{15} ;(e) XRD patterns of Recycled Vc-OCN_{15}.

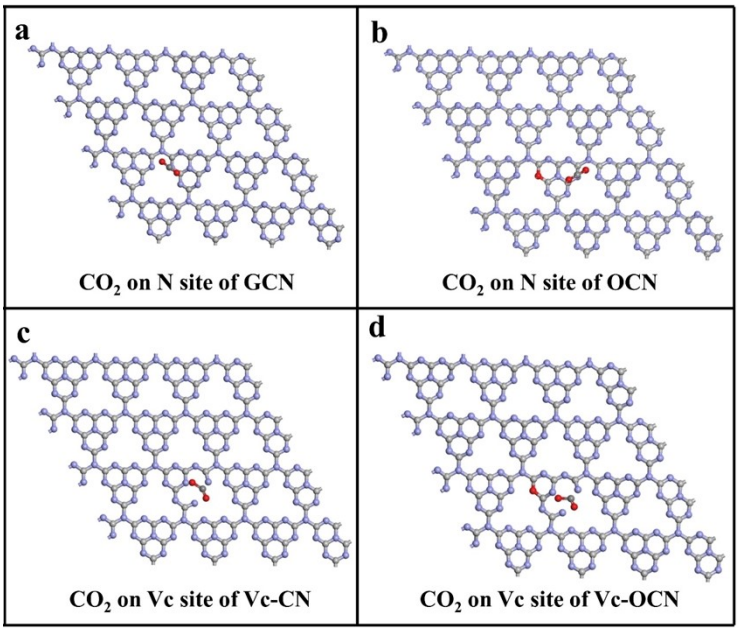

Fig. S12 The optimized models of CO_2 adsorbed on different catalyst and sits. (a) CO_2 adsorbed on N site of GCN, (b) CO_2 adsorbed on N site of OCN, (c) CO_2 adsorbed on Vc site of Vc-CN, (d) CO_2 adsorbed on Vc site of Vc-OCN. The blue, red, and grey ball represent N, O, C atom, respectively.

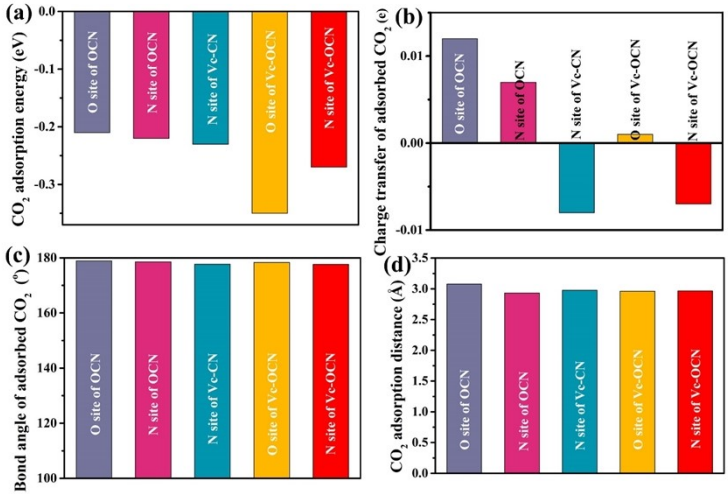

Fig. S13 (a) adsorption energy, (b) charge transfer quantity, (c) bond angle and (d) adsorption distance of CO_2 adsorbed O site of OCN, N site of OCN, N site of Vc-CN, O site of Vc-OCN, and N site of Vc-OCN.

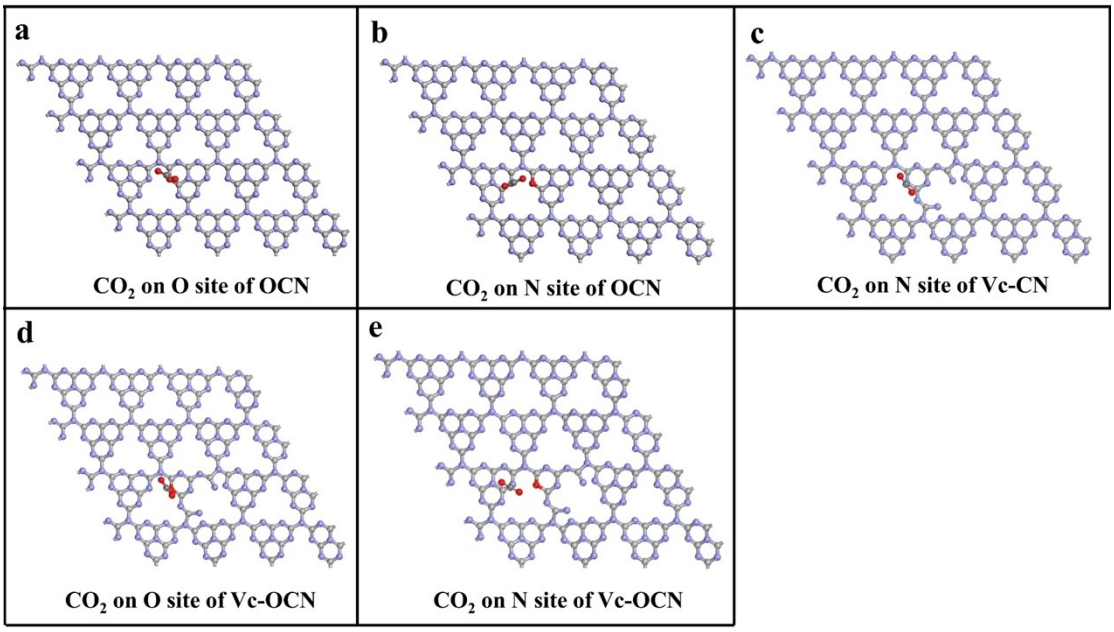

Fig. S14 The optimized models of CO_2 adsorbed on different catalyst and sites. (a) CO_2 adsorbed on O site of OCN, (b) CO_2 adsorbed on N site of OCN, (c) CO_2 adsorbed on N site of Vc-CN, (d) CO_2 adsorbed on O site of Vc-OCN. (e) CO_2 adsorbed on N site of Vc-OCN. The blue, red, and grey ball represent N, O, C atom, respectively.

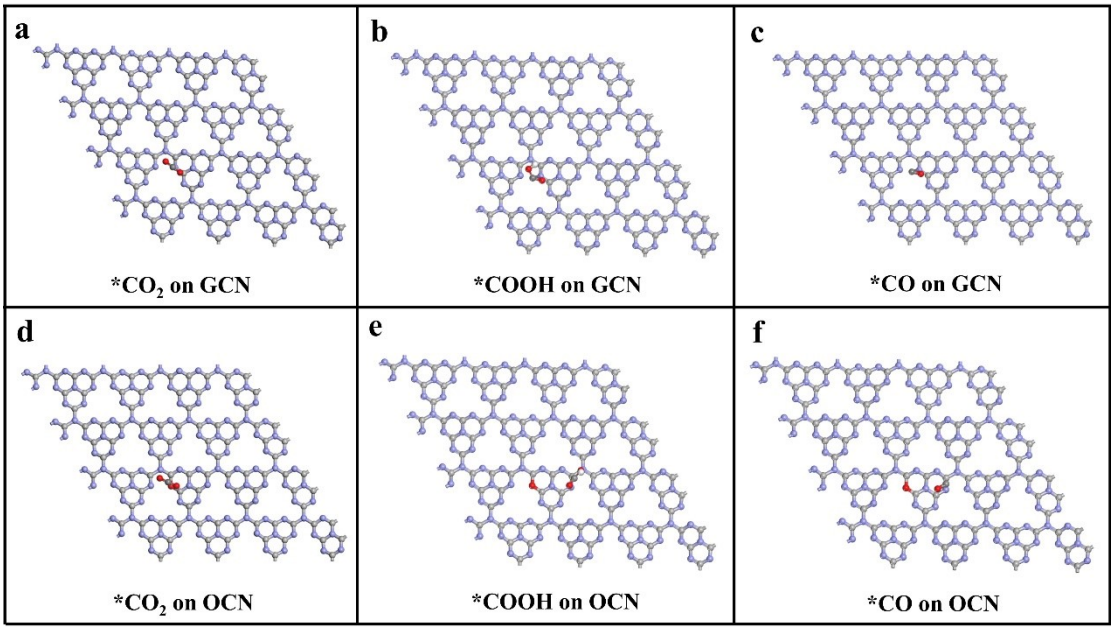

Fig. S15 Optimized model of intermediates *CO_2 on GCN (a), *COOH on GCN (b), *CO on GCN (c), *CO_2 on OCN (d), *COOH on OCN (e), *CO on OCN (f), respectively. The blue, red, and grey ball represent N, O, C atom, respectively.

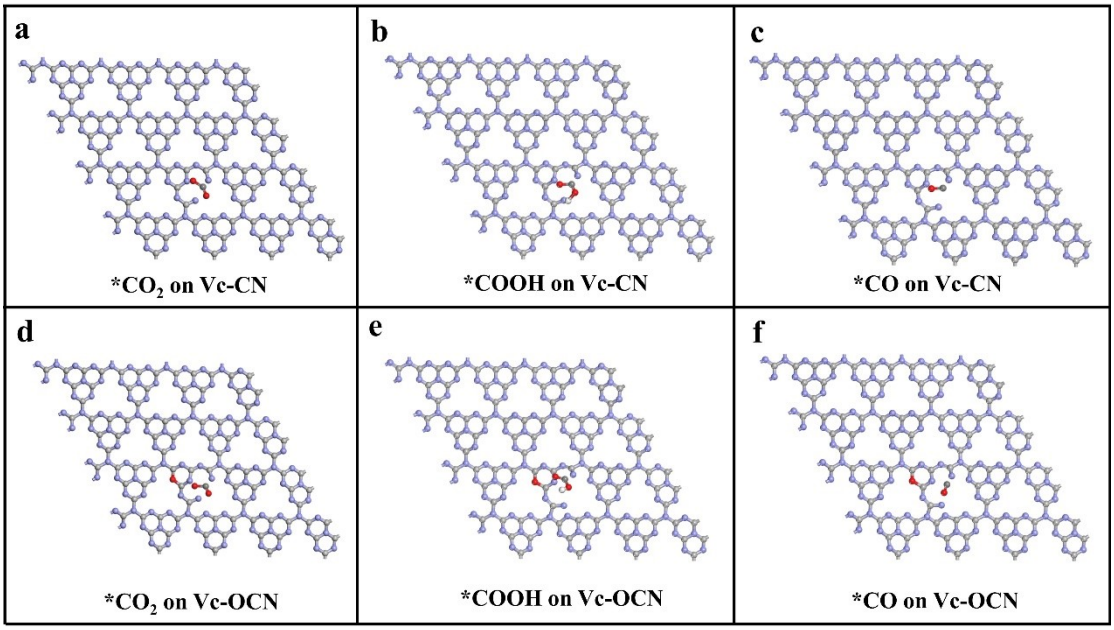

Fig. S16 Optimized model of intermediates *CO_2 on Vc-CN (a), *COOH on Vc-CN (b), *CO on Vc-CN (c), *CO_2 on Vc-OCN (d), *COOH on Vc-OCN (e), *CO on Vc-OCN (f), respectively. The blue, red, and grey ball represent N, O, C atom, respectively.

Table S1. BET surface area of different samples.[a]

Samples	Specific surface areas (m^2/g)
GCN	66.08
OCN	86.86
Vc-OCN	89.45

[a] The specific surface areas are calculated and obtained from the nitrogen adsorption-desorption isotherms.

Table S2. Carbon, nitrogen, and oxygen bonding compositions of various g-C_3N_4 materials (based on XPS analysis)[a].

Sample	C 1s(%)				N 1s(%)			O 1s(%)	
	C-C	C-NH_x	N-C=N	C-O	C-N=C	N-$(C)_3$	NH_x	C-O-C	Adsorbed O
GCN	9.2	2.5	88.3	n.d.	75.3	13.3	11.4	n.d.	100.0
OCN	12.3	2.7	81.3	3.7	73.3	14.1	12.6	57.2	42.8
Vc-OCN_{15}	12.4	4.7	79.1	3.8	73.0	14.0	13.0	56.4	43.6

a) The values in table are obtained by calculating the percentage of the peak area of the selected chemical bond to the total peak area of the corresponding element based on XPS analysis results.

Table S3. Elemental analysis results of carbon, nitrogen and hydrogen in various g-C_3N_4 materials.

Sample	C(wt%)	N(wt%)	H(wt%)	C/N
GCN	34.88	62.41	1.81	0.559
OCN	34.57	61.82	1.83	0.559
Vc-OCN_5	34.19	61.66	1.91	0.554
Vc-OCN_{15}	34.14	61.75	1.95	0.552
Vc-OCN_{50}	33.98	61.79	1.99	0.549

Table S4. The fitting PL decay parameters of GCN, OCN and VC-OCN_{15} [a)] .

Sample	τ1(ns)	*A*1(%)	*t*2(ns)	*A*2(%)	*t*3(ns)	*A*3(%)	*tav(ns)*
GCN	1.59	30.68	6.8	42.1	37.94	27.22	13.68
OCN	1.53	30.01	6.74	43.88	39.2	26.11	13.65
Vc-OCN_{15}	1.76	33.87	7.12	45.01	39.81	21.13	12.21

a)The fitted PL lifetime decay curves [I(t)−t] are based on biexponential decay function (Equation 1)

$I(t) = A1\exp(-t/\tau1) + A2\exp(-t/\tau2) + A3\exp(-t/\tau3)$ (1)

where τ1 and τ2 are the lifetimes of radiative and nonradiative decay components,

A1 and A2 are the amplitudes of radiative and nonradiative decay components.

The average PL lifetime decay (τav) is calculated by Equation 2

$\tau av = (A1\tau1 + A2\tau2 + A3\tau3)/(A1 + A2 + A3)$ (2)

Table S5. The selected results for photocatalytic CO_2 reduction in recent literature

Catalysts	Scavenger	Light source	CO yield (μmol $g^{-1}h^{-1}$)	Refs.
ICN-3	None	300 W, AM1.5	12.09	5
Single Cu atoms/ g-C_3N_4	Ethanol	300 W, Full	3.086	6
Single Ni atoms/g-C_3N_4	Ethanol	300 W, Full	8.6	7
5BSCN	None	300 W, Full	8.2	8
g-C_3N_4 (NH)/COF	TEOA	300 W, λ > 400 nm	11.25	9
LDH/CN/CQDs-6	None	300 W, Full	5.2	10
P-CeO_2/g-C_3N_4	None	300 W, Full	4.18	11
Bi_3O_4Cl/g-C_3N_4	None	300 W, λ > 400 nm	6.6	12
$Cs_2AgBiBr_6$@g-C_3N_4-10%	Methanol	300 W, Full	1.6	13
g-C_3N_4 nanotubes/graphdiyne	None	300 W, λ > 420 nm	7.33	14
K-CN-7	None	300 W, λ > 420 nm	8.7	15
N defect g-C_3N_4	None	4 W ultraviolet (UV) lamp (254 nm, 40 W/cm^2)	8.22	16
Ti_3C_2MXene/g-C_3N_4	None	300 W, λ > 420 nm	5.19	17
Co-MOF/g-C_3N_4	None	300 W, λ > 420 nm	6.75	18
Bi_4NbO_8Cl/g-C_3N_4	None	300 W, Full	2.26	19
g-C_3N_4/$FeWO_4$	Na_2SO_3	300 W, solar simulator	6.12	20
g-C_3N_4@CeO_2	None	300 W, λ > 420 nm	4.2	21
CoZnAl-LDH/RGO/g-C_3N_4	None	300 W, Full	10.11	22
g-C_3N_4/NiAl-LDH	None	300 W, λ > 420 nm	8.2	23
40% NiO/g-C_3N_4	None	300 W, Full	4.17	24
P-g-C_3N_4	None	300 W, Full	2.37	25
Vc-OCN	None	300 W, λ > 400 nm	13.7	This work

Table S6. CO_2 adsorption energy on different models and sites.

Models and sites	Energy (eV)
N site of GCN	-0.27
O site of OCN	-0.21
N1 site of OCN	-0.30
N2 site of OCN	-0.22
Vc site of Vc-CN	-0.57
N site of Vc-CN	-0.23
O site of Vc-OCN	-0.35
Vc site of Vc-OCN	-0.59
N site of Vc-OCN	-0.27

Table S7. CO_2 charge transfer on different models and sites.

Models and sites	charge (e)
N site of GCN	+0.006
O site of OCN	+0.012
N1 site of OCN	+0.007
N2 site of OCN	+0.007
Vc site of Vc-CN	-0.152
N site of Vc-CN	-0.008
O site of Vc-OCN	+0.001
Vc site of Vc-OCN	-0.169
N site of Vc-OCN	-0.007

Table S8. Bond angle of adsorbed CO_2 on different models and sites.

Models and sites	C-O-C angle (°)
N site of GCN	178.56
O site of OCN	178.94
N1 site of OCN	178.88
N2 site of OCN	178.57
Vc site of Vc-CN	135.58
N site of Vc-CN	177.73
O site of Vc-OCN	178.37
Vc site of Vc-OCN	111.46
N site of Vc-OCN	177.66

Table S9. CO_2 adsorption distance on different models and sites.

Models and sites	distance (Å)
N site of GCN	3.077
O site of OCN	3.078
N1 site of OCN	3.066
N2 site of OCN	2.930
Vc site of Vc-CN	2.471
N site of Vc-CN	2.975
O site of Vc-OCN	2.960
Vc site of Vc-OCN	2.132
N site of Vc-OCN	2.966

Reference

1. J. P. Perdew, K. Burke, M. Ernzerhof, Phy. Rev. Lett., 1996, 77, 3865-3868.

2. B. Hammer, L. B. Hansen, J. K. Nørskov, Phy. Rev. B, 1999, 59, 7413-7421.

3. P. E. Blochl, Projector Augmented-Wave Method, Phy. Rev. B, 1994, 50, 17953-17979.

4. G. Kresse, D. Joubert, Phy. Rev. B, 1999, 59, 1758-1775.

5. C. Ban, Y. Duan, Y. Wang, J. Ma, K. Wang, J. Meng, X. Liu, C. Wang, X. Han, G. Cao, L. Gan and X. Zhou, Nano-micro. Lett., 2022, 14, 74.

6. Y. Li, B. Li, D. Zhang, L. Cheng and Q. Xiang, ACS nano, 2020, 14, 10552-10561.

7. L. Cheng, H. Yin, C. Cai, J. Fan and Q. Xiang, Small, 2020, 16, 2002411.

8. Y. Huang, K. Wang, T. Guo, J. Li, X. Wu and G. Zhang, Appl. Catal. B Environ., 2020, 277, 119232.

9. J. Wang, Y. Yu, J. Cui, X. Li, Y. Zhang, C. Wang, X. Yu and J. Ye, Appl. Catal. B Environ., 2022, 301, 120814.

10. W. Liu, Q. Wang, Z. Liu and G. Ding, J. Colloid. Interf. Sci., 2022, 622, 21-30.

11. W. Li, L. Jin, F. Gao, H. Wan, Y. Pu, X. Wei, C. Chen, W. Zou, C. Zhu and L. Dong, Appl. Catal. B Environ., 2021, 294, 120257.

12. Y. Xu, X. Jin, T. Ge, H. Xie, R. Sun, F. Su, X. Li and L. Ye, Chem. Eng. J, 2021, 409, 128178.

13. Y. Wang, H. Huang, Z. Zhang, C. Wang, Y. Yang, Q. Li and D. Xu, Appl. Catal. B Environ., 2021, 282, 119570.

14. C. Sun, Y. Liu, Z. Wang, P. Wang, Z. Zheng, H. Cheng, X. Qin, X. Zhang, Y. Dai and B. Huang, J Alloy. Compd., 2021, 868, 159045.

15. S. Wang, J. Zhan, K. Chen, A. Ali, L. Zeng, H. Zhao, W. Hu, L. Zhu and X. Xu, Acs Sustain., Chem. Eng., 2020, 8, 8214-8222.

16. X. Song, X. Zhang, X. Li, H. Che, P. Huo, C. Ma, Y. Yan and G. Yang, J. Colloid. Interf. Sci., , 2020, 578, 574-583.

17. C. Yang, Q. Tan, Q. Li, J. Zhou, J. Fan, B. Li, J. Sun and K. Lv, Appl. Catal. B Environ., 2020, 268, 118738.

18. Q. Chen, S. Li, H. Xu, G. Wang, Y. Qu, P. Zhu and D. Wang, Chinese J. Catal., 2020, 41, 514-523.

19. Y. Xu, Y. You, H. Huang, Y. Guo and Y. Zhang, J. Hazard. Mater., 2020, 381, 121159.

20. R. Bhosale, S. Jain, C. P. Vinod, S. Kumar and S. Ogale, ACS Appl. Mater. Inter., 2019, 11, 6174-6183.

21. M. Liang, T. Borjigin, Y. Zhang, B. Liu, H. Liu and H. Guo, Appl. Catal. B Environ., 2019, 243, 566-575.

22. Y. Yang, J. Wu, T. Xiao, Z. Tang, J. Shen, H. Li, Y. Zhou and Z. Zou, Appl. Catal. B Environ., 2019, 255, 117771.

23. S. Tonda, S. Kumar, M. Bhardwaj, P. Yadav and S. Ogale, ACS Appl. Mater. Inter., 2018, 10, 2667-2678.

24. J. Tang, R. Guo, W. Zhou, C. Huang and W. Pan, Appl. Catal. B Environ., 2018, 237, 802-810.
25. B. Liu, L. Ye, R. Wang, J. Yang, Y. Zhang, R. Guan, L. Tian and X. Chen, ACS Appl. Mater. Inter., 2018, 10, 4001-4009.